Dalton Transactions

Cite this: *Dalton Trans.*, 2012, **41**, 13308

www.rsc.org/dalton

PAPER

Mixed ligand palladium(II) complexes of 6-methoxy-2-oxo-1,2-dihydroquinoline-3-carbaldehyde 4*N*-substituted thiosemicarbazones with triphenylphosphine co-ligand: Synthesis, crystal structure and biological properties†

Eswaran Ramachandran,[a] Duraisamy Senthil Raja,[a] Nattamai S. P. Bhuvanesh[b] and Karuppannan Natarajan*[a]

Received 18th May 2012, Accepted 26th June 2012
DOI: 10.1039/c2dt31079a

A series of new 6-methoxy-2-oxo-1,2-dihydroquinoline-3-carbaldehyde 4*N*-substituted thiosemicarbazone ligands (**H_2L1–H_2L5**) and their corresponding palladium(II) complexes [Pd(L1)-(PPh_3)] (**1**), [Pd(L2)(PPh_3)] (**2**), [Pd(HL3)(PPh_3)]Cl (**3**), [Pd(L4)(PPh_3)] (**4**) and [Pd(L5)(PPh_3)] (**5**), have been synthesized in order to evaluate the effect of terminal *N*-substitution in thiosemicarbazone moiety on coordination behaviour and biological activity. The new ligands and their corresponding complexes were characterized by analytical and various spectral techniques. The molecular structure of the complexes **2–5** were characterized by single crystal X-ray diffraction studies which revealed that the ligands H_2L2, H_2L4 and H_2L5 are coordinated to palladium(II) as binegative tridentate (ONS^{2-}) by forming six and five member rings whereas, the ligand H_2L3 coordinated to Pd(II) as uninegative tridentate (ONS^{-}). The interactions of the new complexes with calf thymus DNA (CT-DNA) have been evaluated by absorption and ethidium bromide (EB) competitive studies which revealed that complexes **1–5** could interact with CT-DNA through intercalation. Further, the interactions of the complexes with bovine serum albumin (BSA) were also investigated using UV-visible, fluorescence and synchronous fluorescence spectroscopic methods, which showed that the new complexes could bind strongly with BSA. Antioxidant studies showed that all the complexes have a strong antioxidant activity against 2-2′-diphenyl-1-picrylhydrazyl (DPPH) radical and 2,2′-azino-3-ethylbenzthiazoline-6-sulfonic acid diammonium salt (ABTS) cation radical. In addition, *in vitro* cytotoxicity of the complexes against human lung cancer (A549) cell line was assayed which showed that **4** has higher cytotoxic activity than the rest of the complexes and cisplatin.

Introduction

The platinum containing antitumor drugs like cisplatin, carboplatin, and oxaliplatin have widely been used in clinics,[1] but there are limitations due to the drug resistance over a period of time, severe side effects in causing nausea and to the failure of kidney and liver, which are typical of heavy metal toxicity.[2–5] Hence, attempts have been made extensively to replace these drugs with more-efficient, less toxic, and target-specific non-covalent DNA binding anticancer drugs. Since palladium(II) complexes are good alternative candidates for metal–organic antitumor drugs due to their structural and thermodynamic similarities to platinum(II) complexes,[6,7] a number of palladium(II) thiosemicarbazone complexes have been synthesised and examined for their potential as antitumor agents.[8–15] In this area, palladium(II) complexes of heterocyclic thiosemicarbazones have attracted considerable attention and many of them showed remarkable cytotoxic activity.[15,16]

In the recent past, our group has been actively engaged in the study on the variable coordination behaviours of thiosemicarbazones,[17–24] and semicarbazones[25] with diverse transition metals and on the biological properties of the resulting complexes. The results obtained revealed that thiosemicarbazones derived from 2-oxo-1,2-dihydroquinoline-3-carbaldehyde and substituted 2-oxo-1,2-dihydroquinoline-3-carbaldehyde and their transition metal complexes exhibiting significant cytotoxic activities. However, the structural and biological properties of mononuclear palladium complexes of 6-methoxy-2-oxo-1,2-dihydroquinoline-3-carbaldehyde 4*N*-substituted thiosemicarbazone have not been explored. Therefore, it seemed important for us to compare the coordination behaviour and the potential

[a]*Department of Chemistry, Bharathiar University, Coimbatore, 641 046, India. E-mail: k_natraj6@yahoo.com; Fax: +91 422 2422387; Tel: +91 422 2428319*
[b]*Department of Chemistry, Texas A&M University, College Station, TX 77843, USA*

†Electronic supplementary information (ESI) available: Synchronous spectra of BSA (1 μM) in the presence of increasing amounts of the complexes **1** (A), **2** (B), **3** (C), **4** (D) and **5** (E) (0–25 μM) in the wavelength difference of $\Delta\lambda$ = 15 nm and $\Delta\lambda$ = 60 nm (Fig. S1 and S2). CCDC reference numbers 831519, 834540, 880537 and 841993 for the complexes **2**, **3**, **4** and **5**. For ESI and crystallographic data in CIF or other electronic format see DOI: 10.1039/c2dt31079a

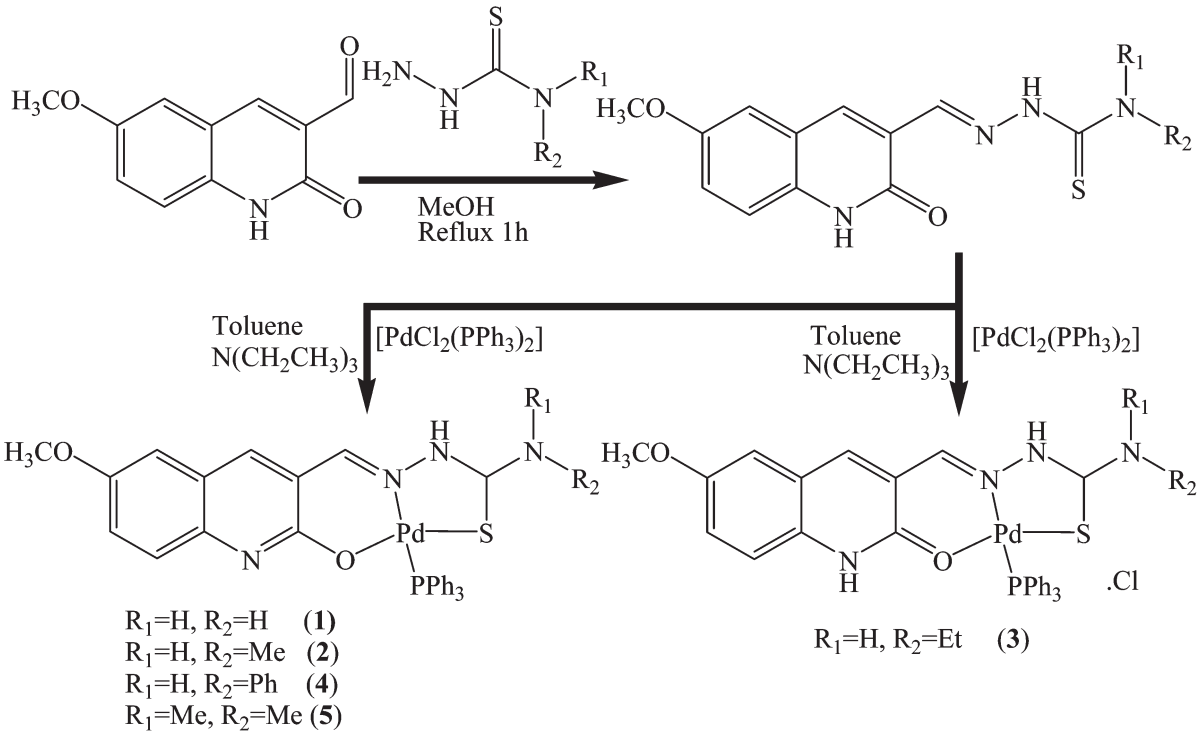

Scheme 1 The synthetic routes of the ligands and its corresponding palladium(II) complexes.

biological activities of mononuclear palladium(II) complexes of 6-methoxy-2-oxo-1,2-dihydroquinoline-3-carbaldehyde 4*N*-substituted thiosemicarbazone.

Herein, we present the synthesis, structure, DNA interaction, protein binding, antioxidative and cytotoxicity studies of mononuclear palladium complexes of 6-methoxy-2-oxo-1,2-dihydroquinoline-3-carbaldehyde 4*N*-substituted thiosemicarbazones. The crystal structures of the new complexes have been determined by X-ray crystallography. The investigation of the biological properties of the new complexes have been carried out focusing on the binding properties with calf thymus DNA (CT-DNA) and competitive binding studies with ethidium bromide (EB). The synthetic routes of the ligands and their corresponding palladium complexes are shown in Scheme 1.

Experimental section

Materials and methods

All the reagents used were of analytical or chemically pure grade. Solvents were purified and dried according to standard procedures.[26] Doubly distilled water was used to prepare buffers. Ethidium bromide (EB), bovine serum albumin (BSA), calf thymus DNA (CT-DNA) and 3-(4,5-dimethylthiazol-2-yl)-2,5-diphenyltetrazolium bromide (MTT) were purchased from Sigma-Aldrich and used as received. 6-Methoxy-2-oxo-1,2-dihydroquinoline-3-carbaldehyde[27] and the starting complex, $[PdCl_2(PPh_3)_2]$[28] were prepared by literature methods. Elemental analyses (C, H, N, S) were performed on a Vario EL III Elementar analyzer instrument. Infrared spectra of the ligand and the metal complexes were recorded in the range of 4000–400 cm^{-1} using a Nicolet Avatar model FT-IR spectrophotometer from KBr discs. The electronic spectra of the complexes were recorded with a Jasco V-630 spectrophotometer using DMSO as the solvent. Emission spectra were measured using a Jasco FP 6600 spectrofluorometer. ^{1}H NMR spectra were recorded on a Bruker AMX 500 at 500 MHz NMR spectrometer using TMS as an internal reference. The melting points were recorded with a Lab India Melting point apparatus.

Synthesis of the ligands

6-Methoxy-2-oxo-1,2-dihydroquinoline-3-carbaldehyde thiosemicarbazone (H_2L1). Thiosemicarbazide (0.911 g, 0.01 mol) dissolved in warm methanol (50 mL) was added to a methanol solution (50 mL) containing 6-methoxy-2-oxo-1,2-dihydroquinoline-3-carbaldehyde (2.032 g, 0.01 mol). The mixture was refluxed for an hour during which period a yellow colour precipitate was formed. The reaction mixture was then cooled to room temperature and the solid compound was filtered. It was then washed with methanol and dried under vacuum. Yield: 86%. MP: 258–260 °C, Elemental Analysis calculated for: $C_{12}H_{12}N_4O_2S$ (%): C, 52.16; H, 4.38; N, 20.28; S, 11.61. Found (%): C, 52.09; H, 4.24; N, 20.31; S,11.56 IR (KBr, cm^{-1}): 3392 (ms) ν(NH); 3160(ms) $\nu(NH_2)$; 1651(s) ν(C═O); 1611, 1530(s) ν(C═N) + ν(C═C); 840(m) ν(C═S). UV-vis (DMSO), λ_{max} (nm): 263, 656, 409 ($\pi \rightarrow \pi^*$, $n \rightarrow \pi^*$). ^{1}H NMR (DMSO-d_6); δ 11.88 (s, N(3)H); 11.62 (s, N(2)H); 8.71 (s, 1H, C(1)H); 8.26–8.29 (d, 2H, N(4)H2); 8.03 (s, 1H, C(6)H); 7.62 (s, 1H, C(10)H); 7.19 (d, 1H, C(7)H); 7.11 (d, 1H, C(8)H); 3.78 (s, 3H, C(11)H).

6-Methoxy-2-oxo-1,2-dihydroquinoline-3-carbaldehyde-4*N*-methylthiosemicarbazone (H_2L2). It was prepared using the same procedure as described for H_2L1 with 4-methyl-3-thiosemicarbazide (1.052 g, 0.01 mol) and 6-methoxy-2-oxo-1,2-dihydroquinoline-3-carbaldehyde (2.032 g, 0.01 mol). A yellow coloured product was obtained. Yield: 83%. MP: 271–273 °C, Elemental Analysis calculated for: $C_{13}H_{14}N_4O_2S$ (%): C, 53.79; H, 4.86; N, 13.30; S, 11.04. Found (%): C, 53.71; H, 4.79; N, 13.43; S, 11.17. IR (KBr, cm^{-1}): 3372(ms) ν(NH); 1658(s) ν(C═O); 1551(s) ν(C═N) + ν(C═C); 856 (m) ν(C═S). UV-vis (DMSO), λ_{max} (nm): 264, 352, 409 ($\pi \rightarrow \pi^*$, $n \rightarrow \pi^*$). ^{1}H NMR (DMSO-d_6); δ 11.90 (s, N(3)H); 11.68 (s, N(2)H); 8.63 (s, 1H, C(1)H); 8.55 (s, 1H, N(4)H); 8.27 (s, 1H, C(6)H); 7.27 (s, 1H, C(10)H); 7.19 (d, 1H, C(7)H); 7.12 (d, 1H, C(8)H); 3.79 (s, 3H, C(11)H); 3.05 (s, 3H, C(13)H).

6-Methoxy-2-oxo-1,2-dihydroquinoline-3-carbaldehyde-4*N*-ethylthiosemicarbazone (H_2L3). It was prepared using the same procedure as described for H_2L1 with 4-ethyl-3-thiosemicarbazide (1.192 g, 0.01 mol) and 6-methoxy-2-oxo-1,2-dihydroquinoline-3-carbaldehyde (2.032 g, 0.01 mol). An yellow colour product was obtained. Yield: 89%. MP: 275–277 °C, Elemental Analysis calculated for $C_{14}H_{16}N_4O_2S$ (%): C, 55.25; H, 5.30; N, 18.41; S, 10.54. Found (%): C, 55.37; H, 5.21; N, 18.38; S, 10.61. IR (KBr, cm^{-1}): 3158 (ms) ν(NH); 1649 (s) ν(C═O); 1621, 1536 (s) ν(C═N) + ν(C═C); 825 (m) ν(C═S). UV-vis (DMSO), λ_{max} (nm): 263, 354, 410 ($\pi \rightarrow \pi^*$, $n \rightarrow \pi^*$). ^{1}H NMR (DMSO-d_6); δ 11.90 (s, N(3)H); 11.61 (s, N(2)H); 8.62 (s, 1H, C(1)H); 8.57 (s, 1H, N(4)H); 8.28 (s, 1H, C(6)H); 7.27 (s, 1H, C(10)H); 7.18 (d, 1H, C(7)H); 7.15 (d, 1H, C(8)H); 3.80 (s, 3H, C(11)H); 3.63 (q, 2H, C(13)H); 1.19 (t, 3H, C(14)H).

6-Methoxy-2-oxo-1,2-dihydroquinoline-3-carbaldehyde-4*N*-phenylthiosemicarbazone (H_2L4). It was prepared using the same procedure as described for H_2L1 with 4-phenyl-3-thiosemicarbazide (1.672 g, 0.01 mol) and 6-methoxy-2-oxo-1,2-dihydroquinoline-3-carbaldehyde (2.032 g, 0.01 mol). A yellow coloured product was obtained. Yield: 92%. MP: 284–286 °C, Elemental Analysis calculated for: $C_{18}H_{16}N_4O_2S$ (%): C, 61.35; H, 4.58; N, 15.90; S, 9.10. Found (%): C, 61.21; H, 4.49; N, 15.79; S, 9.27. IR (KBr, cm^{-1}): 3301(ms) ν(NH); 1656 (s) ν(C═O); 1619, 1539 (s) ν(C═N) + ν(C═C); 837(m) ν(C═S). UV-vis (DMSO), λ_{max} (nm): 264, 354, 413 ($\pi \rightarrow \pi^*$, $n \rightarrow \pi^*$). ^{1}H NMR (DMSO-d_6); δ 12.06 (s, N(3)H); 11.97 (s, N(2)H); 10.15 (s, 1H, C(1)H); 8.84 (s, 1H, N(4)H); 8.42 (s, 1H, C(6)H); 7.27 (m, 8H, aromatic); 3.78 (s, 3H, C(11)H).

6-Methoxy-2-oxo-1,2-dihydroquinoline-3-carbaldehyde-4(*N*,*N*)-dimethylthiosemicarbazone (H2L5). It was prepared using the same procedure as described for H_2L1 with 4,4-dimethyl-3-thiosemicarbazide (1.192 g, 0.01 mol) and 6-methoxy-2-oxo-1,2-dihydroquinoline-3-carbaldehyde (2.032 g, 0.01 mol). A yellow coloured product was obtained. Yield: 86%. MP: 294–296 °C, Elemental Analysis calculated for $C_{14}H_{16}N_4O_2S$ (%): C, 55.25; H, 5.30; N, 18.41; S, 10.54. Found (%): C, 55.31; H, 5.24; N, 18.37; S,10.68. IR (KBr, cm^{-1}): 3427(ms) ν(NH); 1648(s) ν(C═O); 1601, 1510(s) ν(C═N) + ν(C═C); 865(m) ν(C═S). UV-vis (DMSO), λ_{max} (nm): 261, 301, 411 ($\pi \rightarrow \pi^*$, $n \rightarrow \pi^*$).^{1}H NMR (DMSO-d_6); δ 11.87 (s, N(3)H); 11.10 (s, N(2)H); 8.46 (s, 1H, C(1)H); 8.30(s, 1H, C(6)H); 7.37 (d, 1H, C(7)H); 7.26 (s, C(10)H). 7.16–7.17 (d, 1H, C(8)H); 3.78 (s, 3H, C(11)H); 2.49 (s, 6H, C(13, 14)H).

Synthesis of complexes

[Pd(L1)(PPh_3)] (1). To a solution of [$PdCl_2(PPh_3)_2$] (0.100 g; 0.143 mmol) in toluene (20 cm^3), the ligand, **H_2L1** (0.040 g; 0.143 mmol) and two drops of triethylamine were added. The mixture was heated under reflux for 5 h. The resulting solution on slow evaporation yielded an orange coloured crystalline powder. It was washed with toluene and dried under vacuum. The crystals obtained were found to be not suitable for X-ray diffraction. Yield: 79%, MP: 275–277 °C. Anal. calcd for $C_{30}H_{25}N_4O_2PPdS$ (%): C, 56.04; H, 3.92; N, 8.71; S, 4.99; Found (%): C, 56.19; H, 3.86; N, 8.64; S, 4.81. IR (KBr disks, cm^{-1}): 3244(m) ν(NH_2); 1606, 1547 (s) ν(C═N) + ν(C═C); 1354 (s) ν(C–O); 746 (m) ν(C–S); 1445, 1096, 695 (for PPh_3), UV-vis (DMSO), λ_{max} (nm): 268 (intra-ligand transition); 385 (LMCT s/d); 433 (MLCT). ^{1}H NMR (DMSO-d_6); δ 8.52 (s, 1H, C(1)H); 8.49 (s, 1H, C(6)H); 7.15–7.71 (m, 18H, aromatic); 6.98 (s, 2H, N(4)H2); 3.81 (s, 3H, C(11)H).

[Pd(L2)(PPh_3)] (2). It was prepared using the same procedure as described for **1** by the reaction of [$PdCl_2(PPh_3)_2$] (0.100 g; 0.127 mmol) with ligand, **H_2L2** (0.042 g; 0.143 mmol). Dark orange coloured crystals obtained were found to be suitable for X-ray diffraction. Yield: 75%, MP: 254–256 °C, Elemental Analysis calculated for $C_{31}H_{27}N_4O_2PPdS$ (%): C, 56.61; H, 4.25; N, 8.52; S, 4.87; Found (%): C, 56.75; H, 4.32; N, 8.45; S, 4.73. IR (KBr disks, cm^{-1}): 3179 (m) ν(NH); 1598, 1550 (s) ν(C═N) + ν(C═C); 1344 (s) ν(C–O); 747 (m) ν(C–S); 1434, 1098, 693 (for PPh_3), UV-vis (DMSO), λ_{max} (nm): 274(intra-ligand transition); 401 (LMCT s/d); 459 (MLCT). ^{1}H NMR (DMSO-d_6); δ 8.67 (s, 1H, C(1)H); 8.62 (s, 1H, N(4)H); 8.38 (s, 1H, C(6)H); 7.22–7.73 (m, 18H, aromatic); 3.82 (s, 3H, C(11)H); 2.75 (s, 3H, C(13)H).

[Pd(HL3)(PPh_3)]Cl (3). It was prepared as described for **1** by the reaction of [$PdCl_2(PPh_3)_2$] (0.100 g; 0.143 mmol) with ligand, **H_2L3** (0.044 g; 0.143 mmol). Dark orange coloured precipitate formed was filtered and crystals were grown from DMF, found to be suitable for X-ray diffraction. Yield: 81%, MP: 263–265 °C, Elemental Analysis calculated for $C_{32}H_{30}ClN_4O_2PPdS$ (%): C, 54.32; H, 4.27; N, 7.92; S, 4.53; Found (%): C, 54.39; H, 4.39; N, 7.65; S, 4.47. IR (KBr disks, cm^{-1}): 3300(m) ν(NH_2); 1646 (s) ν(C═O); 1608, 1551 (s) ν(C═N) + ν(C═C); 746 (m) ν(C–S); 1434, 1097, 692 (for PPh_3), UV-vis (DMSO), λ_{max} (nm): 276(intra-ligand transition); 415 (LMCT s/d); 437 (MLCT). ^{1}H NMR (DMSO-d_6); δ 12.40 (s, N(3)H); 8.73 (s, 1H, C(1)H); 8.54 (s, 1H, N(4)H); 8.44 (s, 1H, C(6)H); 7.63–7.99 (m, 18H, aromatic); 3.79 (s, 3H, C(11)H); 3.57 (q, 2H, C(13)H); 1.17 (t, 3H, C(14)H).

[Pd(L4)(PPh_3)] (4). It was prepared as described for **1** by the reaction of [$PdCl_2(PPh_3)_2$] (0.100 g; 0.143 mmol) with ligand, **H_2L4** (0.050 g; 0.143 mmol). Dark orange coloured precipitate formed was filtered and the crystals were grown from acetone–DMF solution, found to be suitable for X-ray diffraction. Yield: 84%, MP: 218–220 °C, Elemental Analysis calculated for

Table 1 Experimental data for crystallographic analyses

	Complex **2**	Complex **3**	Complex **4**	Complex **5**
CCDC deposit number	831519	834540	880537	841993
Empirical formula	$C_{31}H_{27}N_4O_2PPdS$	$C_{35}H_{38.11}ClN_5O_{3.56}PPdS$	$C_{42}H_{41}N_4O_4PPdS$	$C_{32}H_{29}N_4O_2PPdS$
Formula weight	657.00	790.62	835.22	671.02
Temperature	110(2) K	110(2) K	110(2) K	110(2) K
Wavelength	0.71073 Å	1.54178 Å	1.54178 Å	1.54178 Å
Crystal system	Monoclinic	Monoclinic	Triclinic	Triclinic
Space group	$P2(1)/c$	$P2(1)/c$	$P\bar{1}$	$P\bar{1}$
Unit cell dimensions				
a (Å)	14.2896(12)	13.110(2)	12.2382(5)	09.8863(3)
b (Å)	11.4236(10)	12.080(2)	12.4005(5)	11.3723(4)
c (Å)	18.1864(15)	24.071(4)	13.5466(5)	13.9140(5)
α(°)	90	90	67.059(2)	101.755(2)
β(°)	109.9050(10)	113.173(11)	80.237(2)	105.532(2)
γ(°)	90	90	81.519(2)	103.784(2)
Volume	2791.4(4) Å^3	3504.5(10) Å^3	1858.29(13) Å^3	1402.71(8) Å^3
Z	4	4	2	2
Density (calculated)	1.563 Mg m^{-3}	1.498 Mg m^{-3}	1.493 Mg m^{-3}	1.589 Mg m^{-3}
Absorption coefficient	0.834 mm^{-1}	6.324 mm^{-1}	5.356 mm^{-1}	6.879 mm^{-1}
F(000)	1336	1622	860	684
Crystal size (mm^3)	0.17 × 0.13 × 0.02	0.50 × 0.04 × 0.04	0.10 × 0.09 × 0.02	0.05 × 0.04 × 0.03
Theta range for data collection	2.14 to 27.49°	4.00 to 59.99°	3.68 to 59.99°	3.44 to 59.99°
Index ranges	$-18 \le h \le 18$ $-14 \le k \le 14$ $-23 \le l \le 23$	$-14 \le h \le 14$ $-13 \le k \le 13$ $-26 \le l \le 26$	$-13 \le h \le 13$ $-13 \le k \le 13$ $-15 \le l \le 15$	$-11 \le h \le 11$ $-12 \le k \le 12$ $-15 \le l \le 15$
Reflections collected	31 688	46 209	41 891	31 583
Independent reflections	6377 [R(int) = 0.0375]	5163 [R(int) = 0.0590]	5379 [R(int) = 0.0571]	4078 [R(int) = 0.0459]
Completeness to θ = 27.49°	99.4%	99.3%	97.7%	98.0%
Absorption correction	Semi-empirical from equivalents	Semi-empirical from equivalents	Semi-empirical from equivalents	Semi-empirical from equivalents
Max. and min. transmission	0.9868 and 0.8712	0.7860 and 0.1441	0.9004 and 0.6165	0.8202 and 0.7248
Data/restraints/parameters	6377/0/363	5163/0/437	5379/18/471	4078/0/373
Goodness-of-fit on F^2	1.037	1.014	1.099	1.054
Final R indices [$I > 2\sigma(I)$]	R_1 = 0.0262 wR_2 = 0.0613	R_1 = 0.0355 wR_2 = 0.0895	R_1 = 0.0355 wR_2 = 0.0969	R_1 = 0.0224 wR_2 = 0.0544
R indices (all data)	R_1 = 0.0350 wR_2 = 0.0657	R_1 = 0.0452 wR_2 = 0.0915	R_1 = 0.0397 wR_2 = 0.0987	R_1 = 0.0250 wR_2 = 0.0550
Largest diff. peak and hole (e Å^{-3})	0.586 and −0.475	1.043 and −0.831	0.830 and −0.728	0.302 and −0.543

$C_{36}H_{29}N_4O_2PPdS$ (%): C, 60.13; H, 4.06; N, 7.79; S, 4.46; Found (%): C, 60.07; H, 4.11; N, 7.83; S, 4.51. IR (KBr disks, cm^{-1}): 3260 (m) ν(NH); 1614, 1561 (s) ν(C═N) + ν(C═C); 1315 (s) ν(C–O); 746 (m) ν(C–S); 1436, 1095, 691 (for PPh_3), UV-vis (DMSO): λ_{max} (nm): 270 (intra-ligand transition); 483 (LMCT s/d); 465 (MLCT). ^{1}H NMR (DMSO-d_6); δ 8.92 (s, 1H, C(1)H); 8.67 (s, 1H, N(4)H); 8.38 (s, 1H, C(6)H); 7.27–7.78 (m, 23H, aromatic); 3.81 (s, 3H, C(11)H).

[Pd(L5)(PPh$_3$)] (5). It was prepared as described for **1** by the reaction of $[PdCl_2(PPh_3)_2]$ (0.100 g; 0.143 mmol) with ligand, **H$_2$L5** (0.044 g; 0.143 mmol). Dark orange coloured crystals obtained were found to be suitable for X-ray diffraction. Yield: 78%, MP: 281–283 °C, Elemental Analysis calculated for $C_{32}H_{29}N_4O_2PPdS$ (%): C, 57.27; H, 4.36; N, 8.35; S, 4.78; Found (%): C, 57.14; H, 4.28; N, 8.25; S, 4.63. IR (KBr disks, cm^{-1}): 3147 (m) ν(NH); 1593, 1550 (s) ν(C═N) + ν(C═C); 1354 (s) ν(C–O); 747 (m) ν(C–S); 1436, 1094, 693 (for PPh_3), UV-vis (DMSO), λ_{max} (nm): 262 (intra-ligand transition); 385 (LMCT s/d); 457 (MLCT). ^{1}H NMR (DMSO-d_6); δ 8.63 (s, 1H, C(1)H); 8.41(s, 1H, C(6)H); 7.12–7.72 (m, 18H, aromatic); 3.84 (s, 3H, C(11)H); 3.05 (s, 6H, C(13, 14)H).

Single crystal X-ray diffraction studies

Single-crystal X-ray diffraction data of complex **2** was collected on a BRUKER APEX 2 X-ray (three-circle) diffractometer, whereas the data for the complexes **3**, **4** and **5** were collected on a BRUKER GADDS X-ray (three-circle) diffractometer at 110 K. Integrated intensity information for each reflection was obtained by reduction of the data frames with APEX2.[29] The integration method employed a three dimensional profiling algorithm and all data were corrected for Lorentz and polarization factors, as well as for crystal decay effects with the program SADABS.[30] The structure of complexes, **2**, **3**, **4** and **5** were solved by direct methods using the program SHELXTL.[31] The refinement and all further calculations were carried out using SHELXTL. The hydrogen atoms bound to carbon were placed in idealized positions and were set riding on the parent atom. Hydrogen atoms attached to N and O were located from the Fourier difference maps and were set riding on the respective

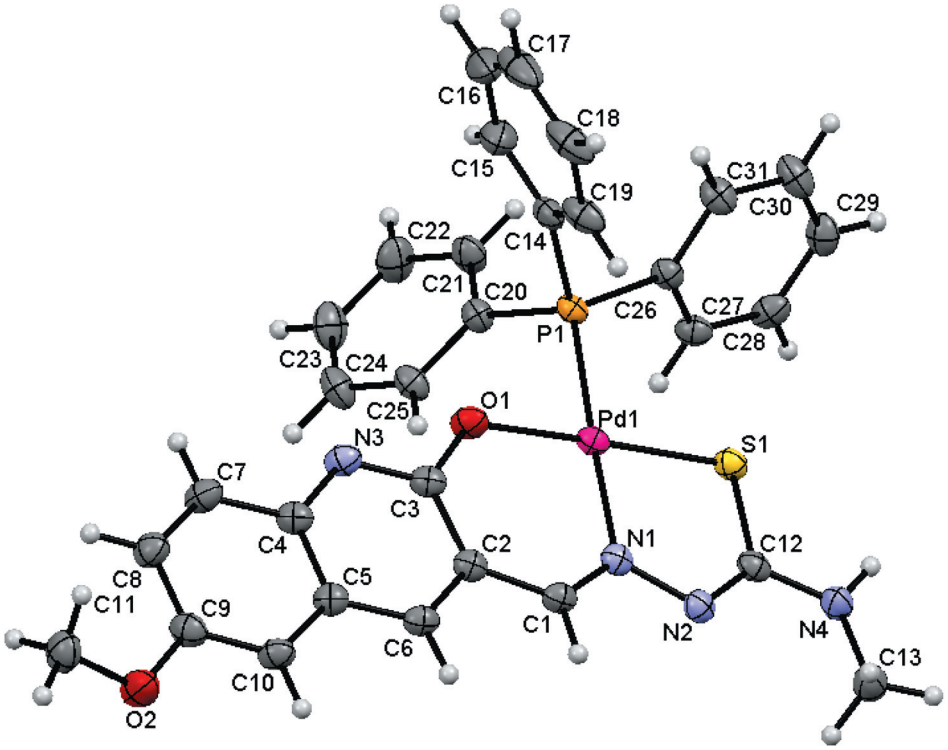

Fig. 1 An ORTEP view of the complex **2** with the atom numbering scheme.

parent atom. All non-hydrogen atoms were refined with anisotropic thermal parameters. A molecule of DMF and water were found solvated in complex **3**. The thermal parameters of O90 (water) indicated that it is partially occupied and the occupancy was refined (0.56). For DMF, the thermal ellipsoids were elongated. A trial to refine the disorder has only increased the number of refinement parameters along with the restraints and did not improve the reliability factors. In complex **4**, two acetone molecules, each disordered between two positions, were found solvated. The structures were refined (weighted least squares refinement on F^2) to convergence.[31] Crystal data and details of structure refinements for complexes are listed in Table 1.

DNA binding experiments

The UV-vis absorption spectroscopic studies and the DNA binding experiments were performed at room temperature. The purity of the CT-DNA was verified by taking the ratio of the absorbance values at 260 and 280 nm in the respective buffer, which was found to be 1.8 : 1, indicating that the DNA was sufficiently free of protein. The DNA concentration per nucleotide was determined by absorption spectroscopy using the molar extinction coefficient value of 6600 $dm^3\ mol^{-1}\ cm^{-1}$ at 260 nm. The complexes were dissolved in a mixed solvent of 5% DMSO and 95% Tris-HCl buffer for all the experiments. Absorption titration experiments were performed with a fixed concentration of the compounds (25 μM) while gradually increasing the concentration of DNA (10–50 μM). While measuring the absorption spectra, an equal amount of DNA was added to both the test solution and the reference solution to eliminate the absorbance of DNA itself.

Further support for the binding of the complexes to DNA *via* intercalation was obtained from emission quenching experiments. For all the experiments, the DNA was pre-treated with ethidium bromide for 30 min. Then the test solutions were added to this mixture of EB-DNA, and the change in the fluorescence intensity was measured. The excitation and the emission wavelength were 515 nm and 613–617 nm, respectively.

Protein binding studies

The excitation wavelength of BSA at 280 nm and the emission at 345 nm were monitored for the protein binding studies. The excitation and emission slit widths and scan rates were maintained constant for all the experiments. Samples were carefully degassed using pure nitrogen gas for 15 min. Quartz cells (4 × 1 × 1 cm) with high vacuum Teflon stopcocks were used for degassing. Stock solution of BSA was prepared in 50 mM phosphate buffer (pH = 7.2) and stored in the dark at 4 °C for further use. Concentrated stock solution of the compounds were prepared as mentioned for the DNA binding experiments except that the phosphate buffer was used instead of Tris-HCl buffer for all the experiments. Titrations were manually done by using a micropipette for the addition of the compounds. For synchronous fluorescence spectra also, the same concentration of BSA and the compounds were used and the spectra were measured at two different $\Delta\lambda$ (difference between the excitation and emission wavelengths of BSA) values such as 15 and 60 nm.

Antioxidant assays

The DPPH radical scavenging activities of the complexes were measured according to the method of Blois.[32] The complexes at

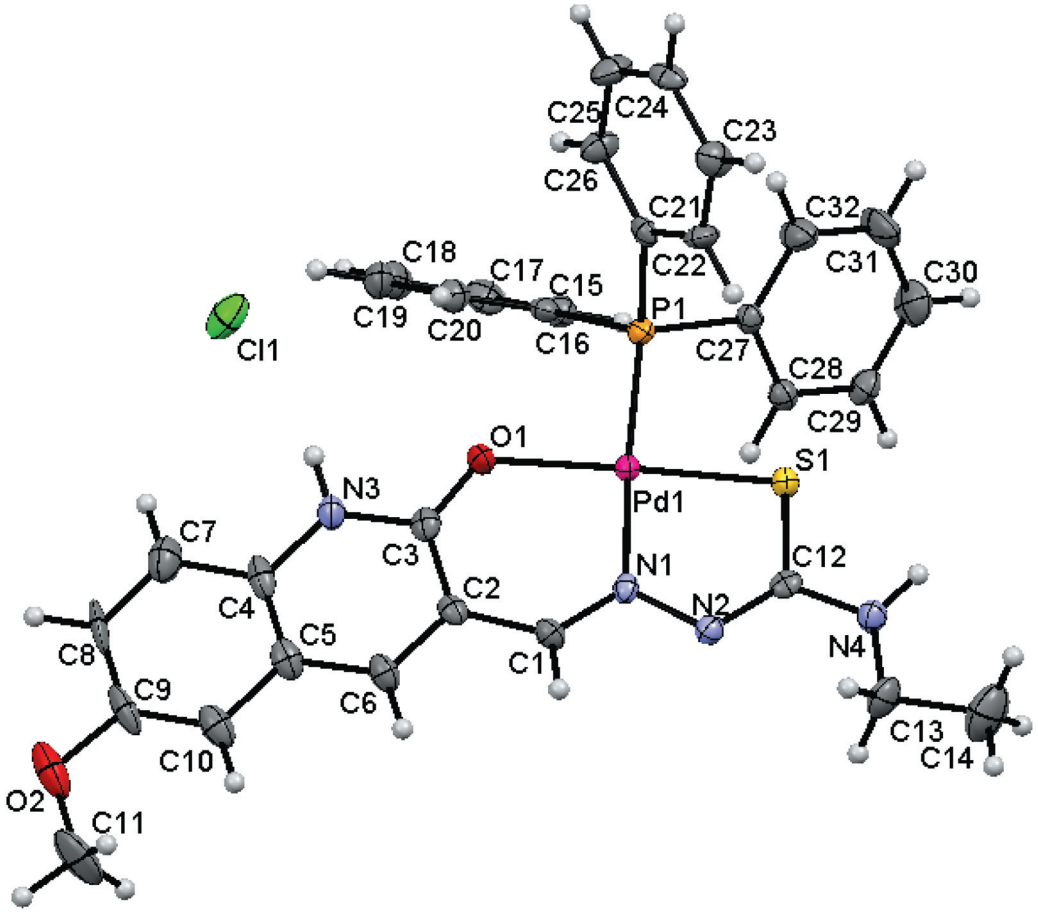

Fig. 2 An ORTEP view of the complex **3** with the atom numbering scheme. The DMF and water molecules are omitted for clarity.

Table 2 Selected bond lengths [Å] and angles [°]

	Complex **2**	Complex **3**	Complex **4**	Complex **5**
Pd(1)–N(1)	2.0262(16)	2.031(3)	2.040(3)	2.024(2)
Pd(1)–O(1)	2.0332(14)	2.063(2)	2.053(3)	2.0393(17)
Pd(1)–S(1)	2.2786(5)	2.2352(10)	2.2167(10)	2.2385(6)
Pd(1)–P(1)	2.2347(6)	2.2775(10)	2.2838(10)	2.2843(7)
N(1)–Pd(1)–O(1)	93.10(6)	92.25(11)	92.43(11)	93.18(7)
N(1)–Pd(1)–S(1)	84.31(5)	84.22(9)	84.07(9)	83.95(6)
O(1)–Pd(1)–S(1)	177.09(4)	175.88(7)	176.16(7)	171.79(5)
N(1)–Pd(1)–P(1)	176.97(5)	175.52(9)	175.23(9)	166.81(6)
O(1)–Pd(1)–P(1)	89.84(4)	91.93(7)	91.11(7)	92.01(5)
S(1)–Pd(1)–P(1)	92.765(19)	91.54(4)	92.30(4)	92.45(2)

various concentrations were taken and the volume was adjusted to 100 µL with methanol. About 5 mL of a 0.1 mM methanolic solution of DPPH was added to the aliquots of compound and standards (BHA, BHT) and shaken vigorously. Negative control was prepared by adding 100 µL of methanol in 5 mL of 0.1 mM methanolic solution DPPH. The tubes were allowed to stand for 20 min at 27 °C. The absorbance of the sample was measured at 517 nm against the blank (methanol). Radical scavenging activity of the samples was expressed as IC_{50} which is the concentration of the compound required to inhibit 50% of DPPH concentration.

The total antioxidant activity of the samples was measured by ABTS radical cation decolorization assay according to the method of Re *et al.*[33] $ABTS^{\cdot+}$ (2,2′-Azino-3-ethylbenzothiazoline-6-sulfonic acid diammonium salt) was produced by reacting 7 mM ABTS aqueous solution with 2.4 mM potassium persulfate in the dark for 12–16 h at room temperature. Prior to assay, this solution was diluted in ethanol (about 1 : 89 v/v) and equilibrated at 30 °C to give an absorbance of 0.700 ± 0.02 at 734 nm. After the addition of 1 mL of diluted ABTS solution to various concentrations of the complexes in ethanol, the absorbance was measured at 30 °C exactly 30 min after the initial mixing.

Cytotoxicity assays

MTT assay. Cytotoxic effect of the compounds on human lung cancer cells (A549) were assayed by the 3-(4,5-dimethylthiazol-2-yl)-2,5-diphenyltetrazolium bromide (MTT) assay.[34] The cells were seeded at a density of 10 000 cells per well in 200 µL and then the compounds were added to the cells at a final concentration of 1, 10, 25 and 50 µM in the cell culture media. After 48 h, the wells were treated with 20 µL MTT (5 mg mL^{-1} PBS) and incubated at 37 °C for 4 h. The purple formazan crystals formed were dissolved in 200 µL DMSO and read at 570 nm in a micro plate reader.

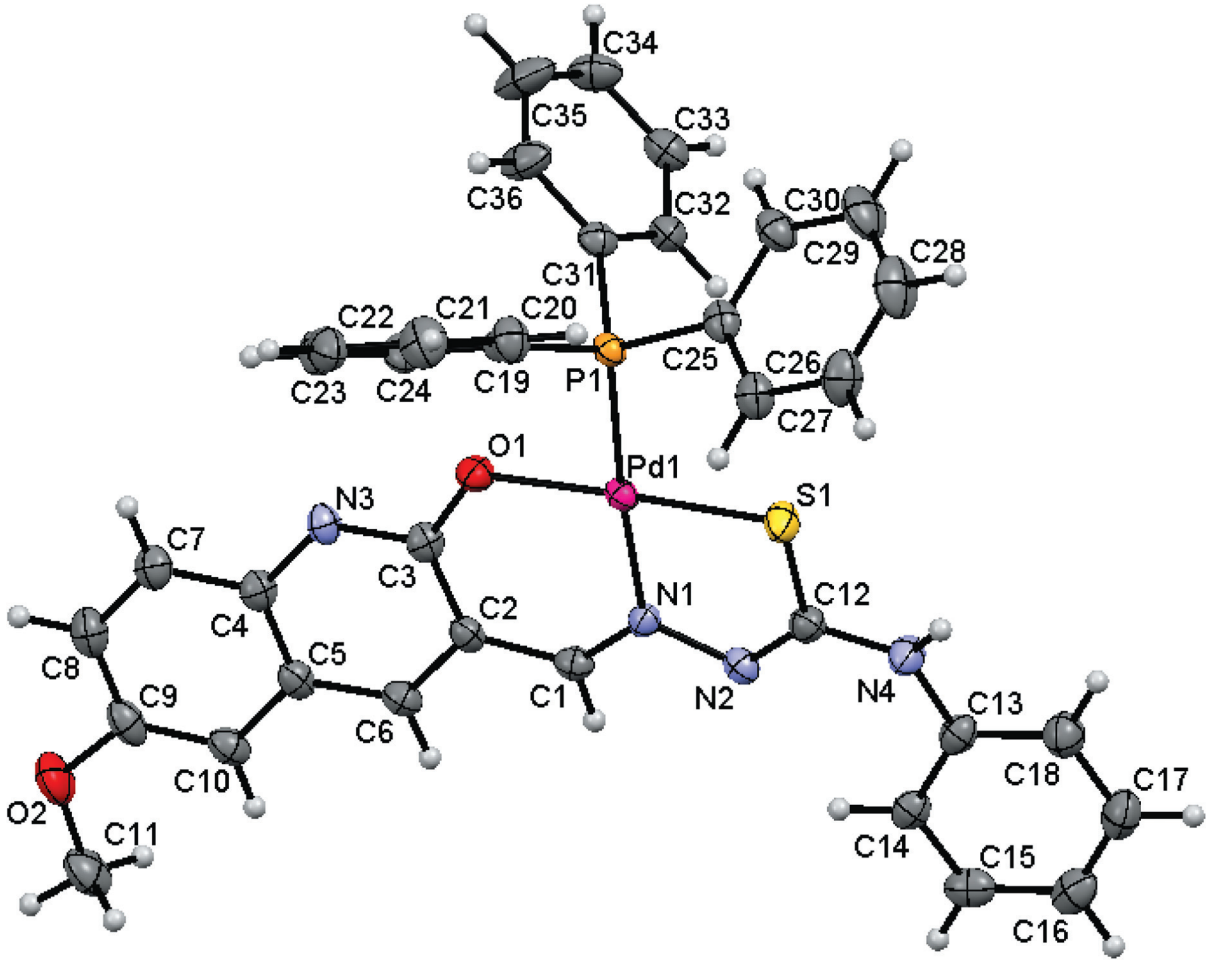

Fig. 3 An ORTEP view of complex **4** with the atom numbering scheme. The distorted DMF molecules are omitted for clarity.

Results and discussion

Synthesis and characterization

The synthetic routes of the ligands and their Pd(II) complexes, **1**, **2**, **3**, **4** and **5** are shown in Scheme 1. The complexes **1–5** were prepared by direct reaction of the corresponding ligand with precursor complex, $[PdCl_2(PPh_3)_2]$ in 1 : 1 mole ratio. While all other ligands coordinated as dibasic tridentate in **1**, **2**, **4** and **5**, the H_2L3 alone coordinated as a monobasic tridentate in **3**. All the new ligands and their mononuclear palladium complexes were characterised by elemental analysis, IR, UV-vis and ^{1}H-NMR spectroscopy and the data are given in the Experimental section. The IR peak shift in ν(C═N), ν(C═O) and ν(C═S) of the ligands in the complexes gave evidence for the coordination of the ligand to palladium ion. In the ^{1}H-NMR spectra of the new complexes the absence of the signal for N(2)H indicated that sulphur coordinated to the palladium ion in the complexes **1–5** in the thiolate form. The absence of the peak for N(3)H in the complexes **1**, **2**, **4** and **5** indicated that the oxygen coordinated to Pd(II) ion as the phenolic form and in complex **3**, the presence of the N(3)H peak clearly indicated that the oxygen coordinated to the palladium in the oxo form. These observations have been confirmed by X-ray single crystal structure analysis. The single crystal X-ray analysis showed that the formulae of the complexes **2**, **4**, **5** and **3** are $[Pd(L)PPh_3]$ and $[Pd(HL)PPh_3]Cl$ respectively. The crystal data, data collection and refinement parameters for the new Pd(II) complexes were summarized in Table 1.

Crystal structures of the complexes 2–5

The molecular structure of the complexes **2** and **3** along with the atomic numbering scheme are given in Fig. 1 and 2. The selected bond lengths and bond angles are summarised in Table 2. The single crystal X-ray diffraction study reveals that complexes **2** and **3** are crystallized in a monoclinic crystal system with the space group *P*2(1)/*c*. In complex **2** the coordination geometry around Pd(II) can be described as a distorted square planar, the palladium atom being bonded to binegative tridentate ONS donor ligand molecules in such a way that five and six membered chelate rings are formed and the remaining site is occupied by triphenylphosphine. In complex **3**, the Pd(II) ions adopt a distorted square planar geometry, the palladium atom being bonded to monobasic tridentate ONS donor ligand molecules and the fourth vacant site is occupied by triphenylphosphine ligand and the complex neutralized by one chlorine atom which is present in lattice. The *trans* angles of O1–Pd1–S1; 177.09(4)° and N–Pd1–P; 166.81(6)° (for **2**) and O(1)–Pd(1)–S(1); 175.88(7)°,

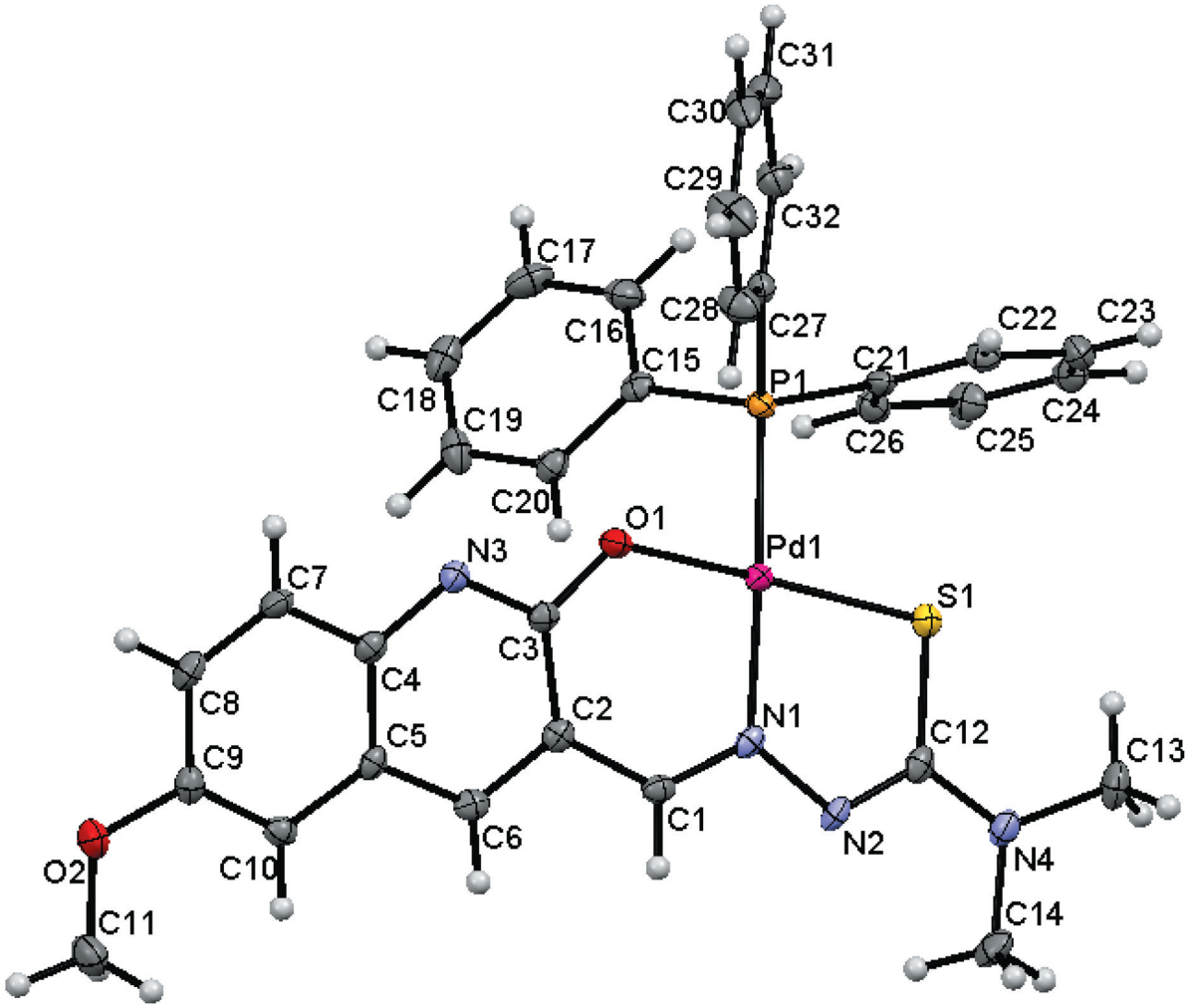

Fig. 4 An ORTEP view of complex **5** with the atom numbering scheme.

N(1)–Pd(1)–P(1); 175.52(9)° (for **3**) indicated a slight deviation from the expected linear *trans* geometry, suggesting distortion in the square planar coordination geometry. The dihedral angle between the mean planes of the coordinating five-member chelation ring and the six member one is 2.18° and 3.97° for **2** and **3** respectively.

The ORTEP view of complexes **4** and **5** along with the coordinating atomic numbering scheme are depicted in Fig. 3 and 4, and selected bond lengths and bond angles are listed in Table 2. The complexes **4** and **5** crystallized in a triclinic system with the space group $P\bar{1}$. In both **4** and **5**, the coordination geometry around Pd(II) is a distorted square planar, the palladium atom being bonded to binegative tridentate ONS donor ligand molecules in such a way that five and six membered chelate rings are formed. The remaining site is occupied by triphenylphosphine. The *trans* angles of complex **4** O1–Pd1–S1; 176.16(7)° and N–Pd1–P; 175.23(9)° and complex **5** are O(1)–Pd(1)–S(1); 171.79(5)° and N(1)–Pd(1)–Cl(1); 166.81(6)° which showed a slight deviation from the expected linear *trans* geometry, suggesting distortion in the square planar coordination geometry. The dihedral angle between the mean planes of the coordinating five-member chelation ring and the six member one is 6.38° and 6.92° for **4** and **5** respectively. The analysis of the bond lengths and angles (Table 2) of the complexes **2–5** gives further support to the belief that the oxo group oxygen of complex **3** bonded to the metal ion in neutral mode and in the rest of the complexes the oxo group oxygen is bonded to the metal ion as O^{-}.

DNA binding studies

DNA binding is the predominant property looked for in pharmacology when evaluating the potential of new antitumor complexes, and hence, the interaction between DNA and the synthesized complexes needs to be investigated. The mode and tendency for the binding of the complexes **1–5** to CT-DNA were studied with different methods.

Electronic absorption titration

Electronic absorption spectroscopy is one of the most useful techniques for the investigation of the mode of interaction of metal complexes with DNA.[35,36] Complexes binding to DNA through intercalation usually results in hypochromism with or

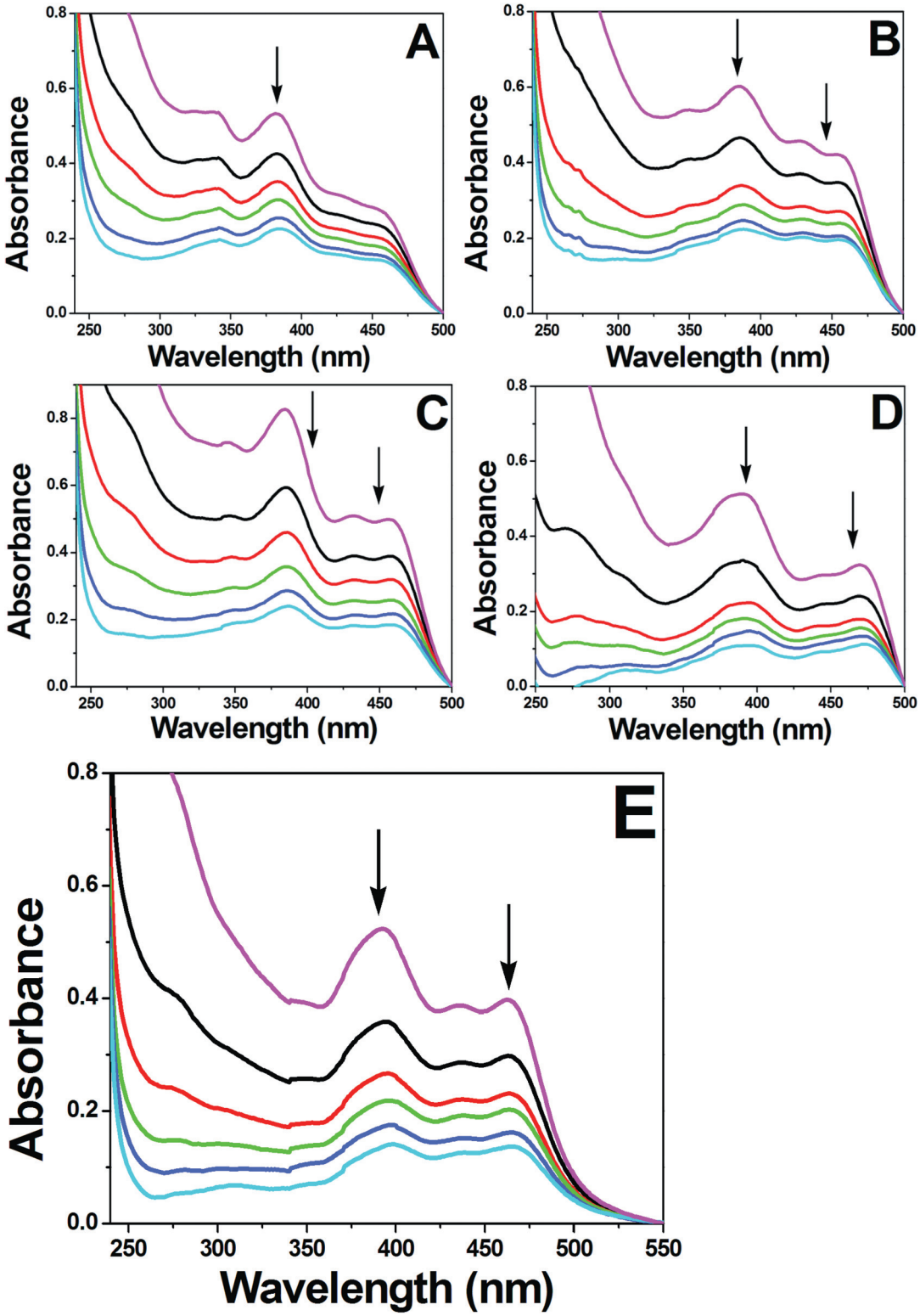

Fig. 5 Electronic spectra of complexes **1** (A), **2** (B), **3** (C), **4** (D) and **5** (E) in Tris-HCl buffer upon addition of CT-DNA. [Complex] = 25 μM, [DNA] = 0–50 μM. Arrow shows the absorption intensities decrease upon increasing DNA concentration.

without a small red or blue shift, since the intercalative mode involves a strong stacking interaction between the planar aromatic chromophore and the base pairs of DNA.[21,37] The results of absorption spectra of complexes in the absence and presence of CT-DNA is given in Fig. 5. Upon increasing the concentration of DNA to the test complexes, the absorption bands of the complexes **1** and **2** exhibited hypochromism of 57.49% and 62.79% and 25.41% with blue shifts of 3 and 4 and 2 nm at 382 and 384

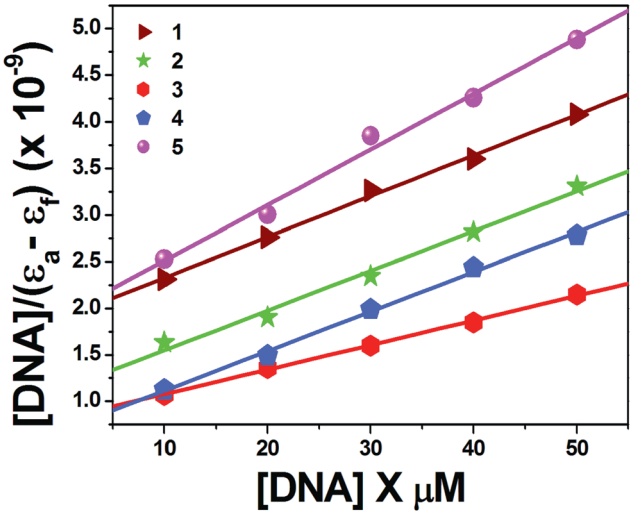

Fig. 6 Plots of $[DNA]/(\varepsilon_a - \varepsilon_f)$ *versus* [DNA] for the complexes **1–5** with CT-DNA.

and 427 nm whereas the absorption bands of complex **3** at 384 and 432 nm exhibited a hypochromism of about 70.30 and 64.08% with blue shifts of 3 and 1 nm. However, complex **4** at 391 nm and 470 nm exhibited a hypochromism of about 80.48% and 68.05% with blue shifts of 4 and 3 nm and complex **5** at 392 and 463 nm exhibited a hypochromism of about 73.03% and 65.49% with blue shifts of 5 and 2 nm, respectively. These results revealed that all the new palladium complexes bind to the DNA helix *via* intercalation, due to stacking interaction between the planar aromatic chromophore and the base pairs of DNA. Complex **4** showed more hypochromicity than the other complexes, indicating that the binding strength of complex **4** is much stronger than the other complexes. In order to further compare the binding strength of the palladium complexes, their intrinsic binding constants (K_b) were determined from the following equation.[38]

$$[DNA]/(\varepsilon_a - \varepsilon_f) = [DNA]/(\varepsilon_b - \varepsilon_f) + 1/K_b(\varepsilon_b - \varepsilon_f)$$

where, [DNA] is the concentration of DNA in the base pairs, ε_a is the apparent absorption coefficient corresponding to A_{obs}/[compound], ε_f is the extinction coefficient of the free compound and ε_b is the extinction coefficient of the compound when fully bound to DNA. From the plot of $[DNA]/(\varepsilon_a - \varepsilon_f)$ *versus* [DNA] (Fig. 6), the intrinsic binding constant K_b was calculated from the ratio of the slope and the intercept. The intrinsic binding constant (K_b) values were 2.31(±0.04) × 10^4 M^{-1}, 3.26(±0.02) × 10^4 M^{-1}, 3.78(±0.07) × 10^4 M^{-1}, 5.46 (±0.05) × 10^5 M^{-1} and 6.18(±0.06) × 10^4 M^{-1} for complexes **1**, **2**, **3**, **4** and **5** respectively. The experimental values of K_b revealed that complexes **1–5** bind to DNA *via* the intercalative mode. From the results obtained, it has been found that complex **4** strongly binds with CT-DNA compared to the remaining complexes, which may be due to the presence of the phenyl ring in the terminal nitrogen of the respective ligand, preferring interaction of the complex with the DNA bases through π–π interaction. From the above experimental studies the order of binding affinity of the complexes is **1** < **2** < **3** < **5** < **4**, though it has been found that complexes **1–5** can bind to DNA by intercalation, the binding mode needs to be proven through further experiments.

Ethidium bromide (EB) displacement studies

The absorption titration results indicate that the complexes effectively bind to DNA. In order to confirm the binding mode and compare their binding affinities, ethidium bromide displacement experiments were carried out. EB is a planar cationic dye which is widely used as a sensitive fluorescence probe for native DNA. EB emits intense fluorescent light in the presence of DNA due to its strong intercalation between the adjacent DNA base pairs.[39,40] Hence, EB displacement technique can provide indirect evidence for the DNA binding mode. The displacement technique is based on the decrease of fluorescence resulting from the displacement of EB from a DNA sequence by a quencher and the quenching is due to the reduction of the number of binding sites on the DNA that is available to EB. Fig. 7 shows the fluorescence quenching spectra of DNA-bound EB by complexes and illustrates that as the concentration of the complexes increases, the emission band at 613 nm exhibited hypochromism up to 14.88, 16.07, 18.15, 20.20 and 21.11% with blue shifts of 3, 2, 4, 4 and 3 nm of the initial fluorescence intensity for **1–5** respectively. The observed decrease in the fluorescence intensity clearly indicates that the EB molecules are displaced from their DNA binding sites and are replaced by the complexes under investigation.[41] The quenching parameter can be analyzed according to the Stern–Volmer equation,

$$F_0/F = K_q\,[Q] + 1$$

where F_0 is the emission intensity in the absence of compound, F is the emission intensity in the presence of compound, K_q is the quenching constant, and $[Q]$ is the concentration of the compound. The K_q value is obtained as a slope from the plot of F_0/F *versus* $[Q]$. From the Stern–Volmer plot (Fig. 8) of F_0/F *versus* $[Q]$, the quenching constants (K_q) were obtained from the slope which were 7.21 × 10^3 M^{-1}, 7.29 × 10^3 M^{-1}, 8.46 × 10^3 M^{-1}, 10.35 × 10^3 M^{-1} and 9.75 × 10^3 M^{-1} respectively for **1–5**. Further, the apparent DNA binding constant (K_{app}) were calculated using the following equation,

$$K_{EB}[EB] = K_{app}[complex]$$

where the compound concentration is the value at a 50% reduction in the fluorescence intensity of EB, K_{EB} (1.0 × 10^7 M^{-1}) is the DNA binding constant of EB, [EB] is the concentration of EB = 12 μM), and they were found to be 8.65 × 10^5 M^{-1}, 8.74 × 10^5 M^{-1}, 10.15 × 10^5 M^{-1}, 12.42 × 10^5 M^{-1} and 11.70 × 10^5 M^{-1} respectively for **1–5**. From these experimental data, it is seen that the order of binding affinities of the complexes is in the order **4** > **5** > **3** > **2** > **1**, which is in agreement with the results observed from the electronic absorption spectra. Furthermore, the observed quenching constants and binding constants of the palladium(II) complexes suggested that the interaction of the complexes **1–5** with DNA should be of intercalation.[23]

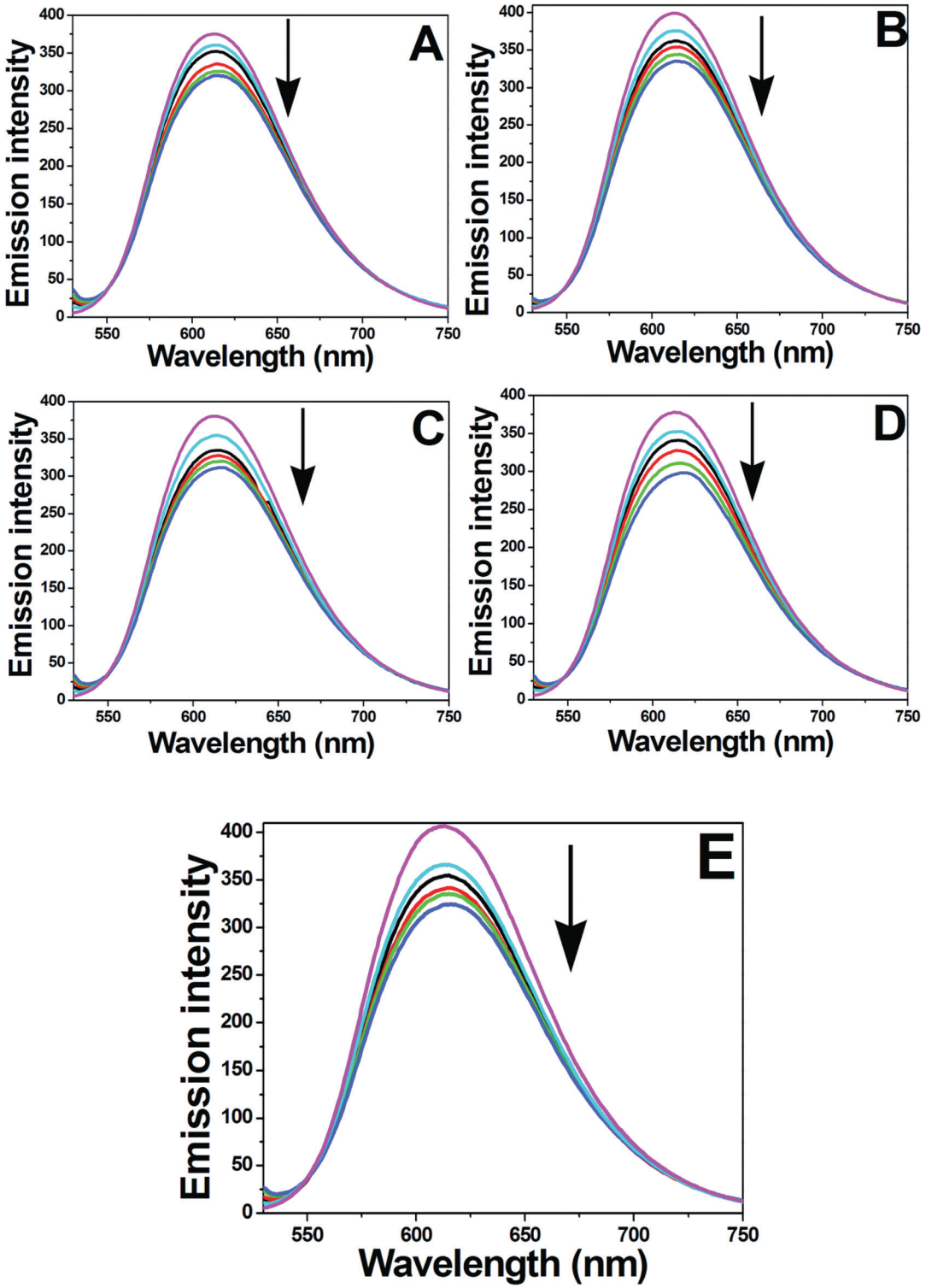

Fig. 7 Fluorescence quenching curves of ethidium bromide bound to DNA: **1** (A), **2** (B), **3** (C), **4** (D) and **5** (E). [DNA] = 12 μM, [EB] = 12 μM, and [complex] = 0–25 μM. Arrow shows the emission intensity changes upon increasing complex concentration.

Protein binding studies

Fluorescence quenching of BSA by mononuclear palladium(II) complexes. It has been proved that the interaction of drugs with blood plasma proteins particularly with serum albumin is involved in the transport of metal ions and metal complexes with drugs through the blood stream. Usually, the binding of drugs to these proteins may lead to either a loss or enhancement of the biological properties of the original drug. Fluorescence spectra are useful in the qualitative analysis of the binding of chemical

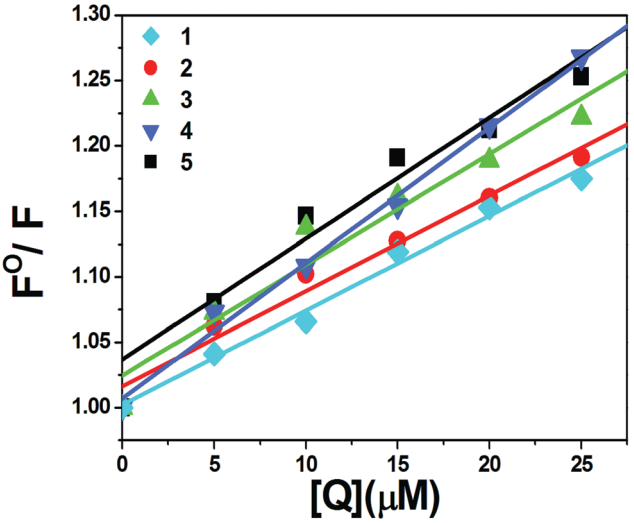

Fig. 8 Stern–Volmer plots of the fluorescence titrations of the complexes **1**, **2**, **3**, **4** and **5**.

compounds to BSA. Generally, the fluorescence of BSA is caused by two intrinsic characteristics of the protein, namely tryptophan and tyrosine. Changes in the emission spectra of tryptophan are observed in response to protein conformational transitions, subunit associations, substrate binding, or denaturation. The intrinsic fluorescence of BSA will provide considerable information on their structure and dynamics and is often utilized in the study of protein folding and association reactions. The interaction of BSA with the complexes was studied by fluorescence measurement at room temperature. A solution of BSA (1 μM) was titrated with various concentrations of the complexes **1–5** (0–25 μM). Fluorescence spectra were recorded in the range of 290–450 nm upon excitation at 280 nm. The effects of the compound on the fluorescence emission spectrum of BSA are given in Fig. 9. Addition of the new complexes to the solution of BSA resulted in a significant decrease of the fluorescence intensity of BSA at 346 nm, up to 79.45, 85.52, 87.49, 89.51 and 87.94% from the initial fluorescence intensity of BSA accompanied by a hypsochromic shift of 1–3 nm for the complexes **1–5** respectively. The observed blue shift is mainly due to the fact that the active site in protein is buried in a hydrophobic environment. These results indicated a definite interaction of all of the complexes with the BSA protein.[22,24]

Furthermore, fluorescence quenching data were analysed with the Stern–Volmer equation and Scatchard equation. From the plot of F_0/F *versus* [Q] the quenching constant (K_q) can be calculated (Fig. 10). If it is assumed that the binding of compounds with BSA occurs at equilibrium, the equilibrium binding constant can be analysed according to the Scatchard equation:

$$\log[I_0 - I/I] = \log K_{bin} + n \log[Q]$$

where K_{bin} is the binding constant of the compound with DNA and n is the number of binding sites. The number of binding sites (n) and the binding constant (K_{bin}) have been found from the plot of $\log(I_0 - I)/I$ *versus* log [Q] (Fig. 11). The calculated K_q, K_{bin}, and n values are given in Table 3. The calculated value of n is around 1 for all of the compounds, indicating the existence of just a single binding site in BSA for all of the compounds. From the values of K_q and K_{bin}, it is inferred that complex **4** interacts with BSA more strongly than the rest of the complexes. Here again, complex **4** shows better activity due to the presence of a phenyl group at the terminal N atom of the coordinated ligand which can interact with the active site by making it more hydrophobic. On decreasing the bulkiness in substitution, the binding constant value (K) also decreases.

Quenching usually occurs either by dynamic or static quenching. Dynamic quenching is a process in which the fluorophore and the quencher come into contact during the transient existence of the excited state. On the other hand, static quenching refers to the formation of a fluorophore–quencher complex in the ground state. A simple method to determine the type of quenching is UV-visible absorption spectroscopy. UV-visible spectra of BSA in the absence and presence of the complexes (Fig. 12) showed that the absorption intensity of BSA was enhanced as the complexes were added, and there was a little blue shift of about 1 nm for all the complexes. It showed that there exists a static interaction between BSA and the added compounds due to the formation of the ground state complex of the type of BSA-compound reported earlier.[41]

Characteristics of synchronous fluorescence spectra

In order to investigate in detail the structural changes which occurred to BSA upon the addition of new compounds, synchronous fluorescence spectra of BSA were measured before and after the addition of test compounds. The results provide reasonable information on the molecular microenvironment, particularly in the vicinity of the fluorophore functional groups.[41] It is a well-known fact that the fluorescence of BSA is normally due to the presence of tyrosine, tryptophan and phenylalanine residues and hence, spectroscopic methods are usually applied to study the conformation of serum protein. According to Miller,[42] the difference between the excitation wavelength and emission wavelength ($\Delta\lambda = \lambda_{emi} - \lambda_{exi}$) indicates the type of chromophore. A higher $\Delta\lambda$ value such as 60 nm is characteristic of the tryptophan residue while a lower $\Delta\lambda$ value such as 15 nm is characteristic of the tyrosine residue.[39] Fig. S1 and S2† show the synchronous fluorescence spectra of BSA with various concentrations of test complexes recorded at $\Delta\lambda$ = 15 nm and $\Delta\lambda$ = 60 nm respectively. In the synchronous fluorescence spectra of BSA at $\Delta\lambda$ = 15, addition of the complexes to the solution of BSA resulted in an increase of the fluorescence intensity of BSA at 302 nm; 1.09, 1.47, 1.51, 2.35 and 1.69 times of the initial fluorescence intensity of BSA for the complexes **1**, **2**, **3**, **4** and **5** respectively. But, in the case of synchronous fluorescence spectra of BSA at $\Delta\lambda$ = 60, addition of the compounds to the solution of BSA resulted in a significant decrease of the fluorescence intensity of BSA at 343 nm, up to 81.14, 82.53, 86.12, 88.53 and 86.56% of the initial fluorescence intensity of BSA accompanied by a trivial blue shift of 1 and 2 nm for complexes **1–5**. The spectral studies clearly suggested that the fluorescence intensities of both the tryptophan and tyrosine were decreased but the emission wavelength of the tryptophan residues is blue shifted with increasing concentration of the complexes. At the same time, there is no change in the emission wavelength of

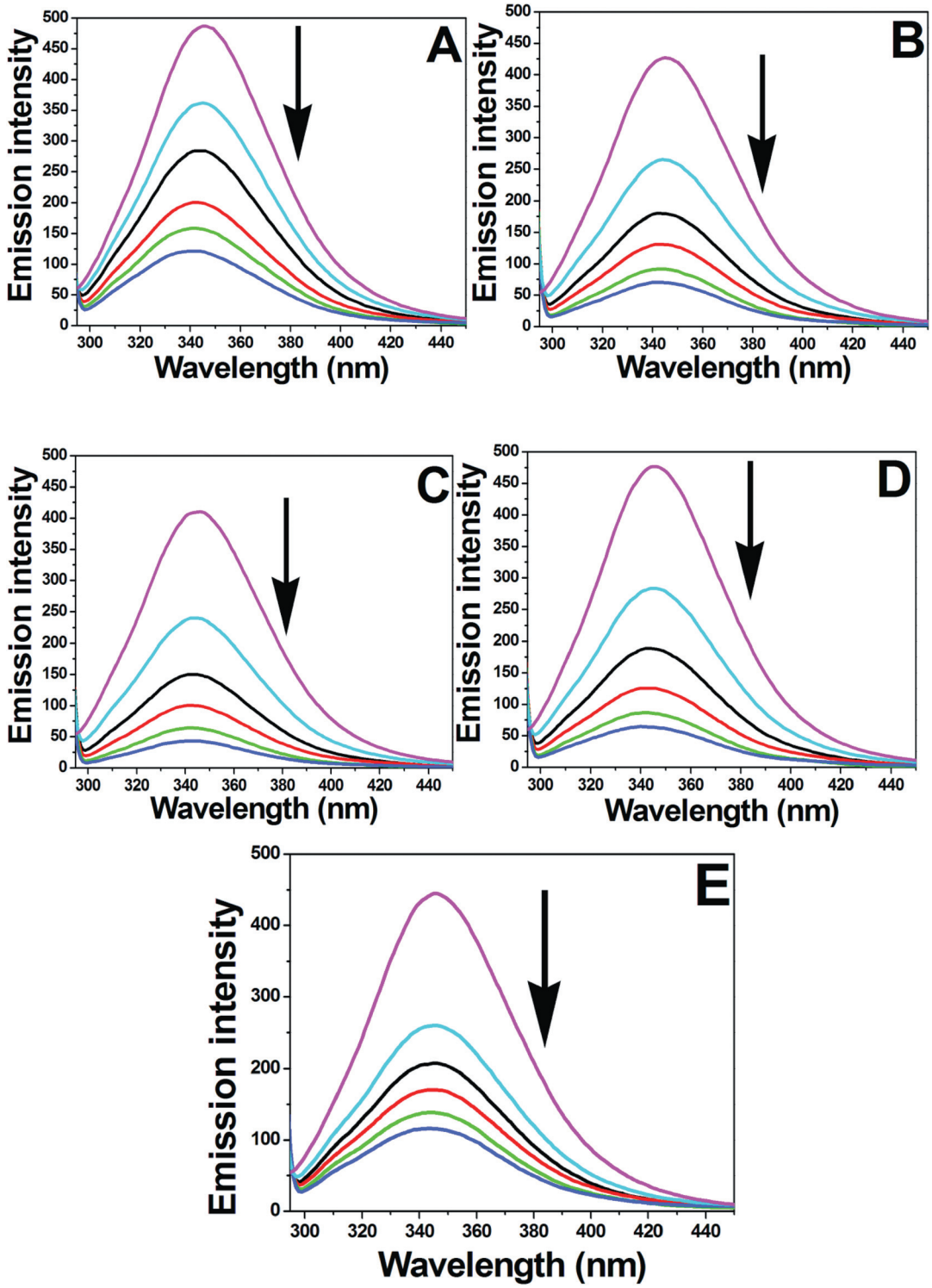

Fig. 9 The emission spectrum of BSA (1 μM; λ_{exi} = 280 nm; λ_{emi} = 346 nm) in the presence of increasing amounts of the complexes **1** (A), **2** (B), **3** (C), **4** (D) and **5** (E) (0–25 μM). Arrow shows the emission intensity changes upon increasing complex concentration.

tyrosine. It suggested that the interaction of compounds with BSA affects the conformation of the tryptophan micro-region.[21] It further indicated that the hydrophobicity around tryptophan residues is strengthened. The hydrophobicity observed in fluorescence and synchronous measurements confirmed the effective binding of all the complexes with the BSA. Hence, the strong interaction of these compounds with BSA suggested that the complexes may be fit for anticancer studies.

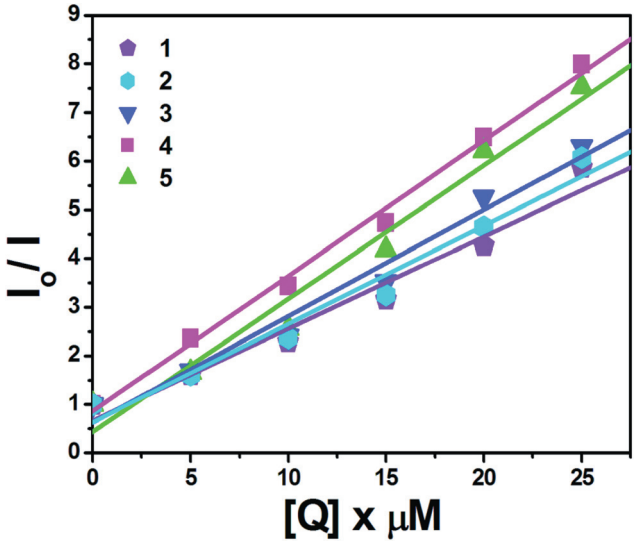

Fig. 10 Stern–Volmer plots of the fluorescence titration of the complexes **1–5** with BSA.

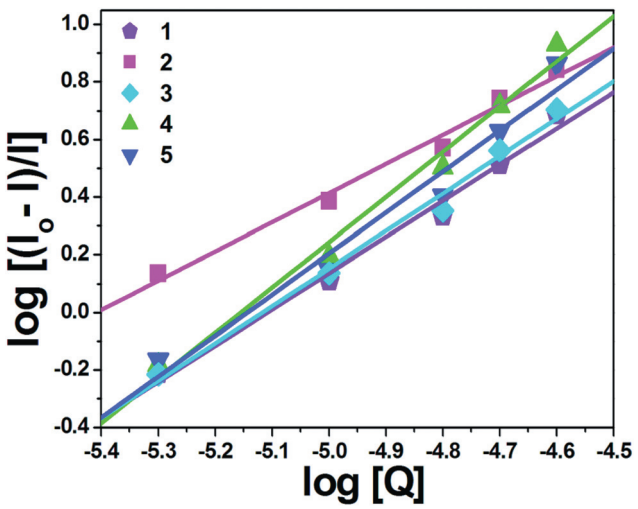

Fig. 11 Scatchard plots of the fluorescence titration of the complexes **1–5** with BSA.

Table 3 Quenching constant (K_q), binding constant (K_{bin}) and number of binding sites (n) for the interactions of complexes with BSA

Complexes	K_q (M^{-1})	K_{bin} (M^{-1})	n
1	$1.89(0.05) \times 10^5$	$03.05(0.04) \times 10^5$	1.01
2	$2.19(0.17) \times 10^5$	$02.66(0.12) \times 10^6$	1.25
3	$2.20(0.17) \times 10^5$	$04.54(0.05) \times 10^6$	1.47
4	$2.78(0.23) \times 10^5$	$12.51(0.09) \times 10^7$	1.52
5	$2.74(0.45) \times 10^5$	$02.12(0.17) \times 10^7$	1.30

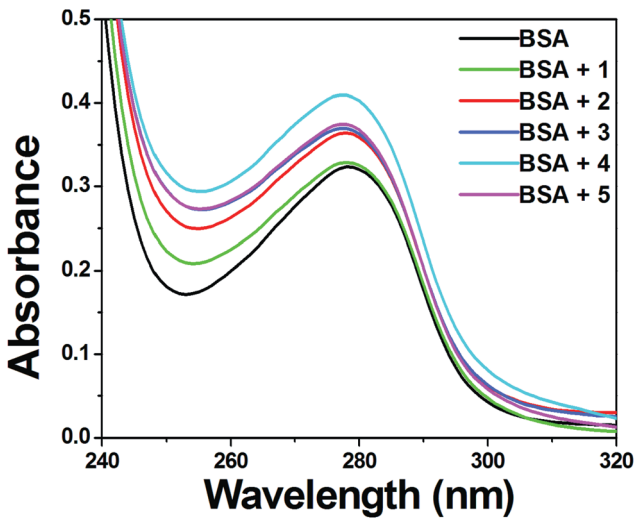

Fig. 12 UV absorption spectra of BSA (10 μM) in the presence of the complex (5 μM).

Table 4 The radical scavenging activity of the complexes

	IC_{50} values (μm)	
Complexes	DPPH$^{\cdot}$	ABTS$^{\cdot}$
Complex **1**	08.56	06.95
Complex **2**	09.45	18.68
Complex **3**	08.62	08.90
Complex **4**	08.38	06.79
Complex **5**	11.95	24.15
BHA	25.58	21.58
BHT	45.99	37.99

Antioxidant activity

Since the palladium complexes exhibited good DNA and protein binding affinity, it was considered meaningful to study the antioxidant activity of these complexes. Hence, a systematic study was carried out on the antioxidant potential of the new complexes along with standards, such as butylated hydroxy anisole (BHA) and butylated hydroxyl toluene (BHT), against DPPH and ABTS radicals with respect to different concentrations of the complexes and the results are shown in Table 4. It is seen from the results that complexes **1–5** possess potent antioxidant activities. However, complex **4** showed better activity than the other four complexes, which may be due to the electron withdrawing effect of the phenyl group on the terminal nitrogen atom of the ligand. It is to be noted that the new palladium(II) complexes showed a better antioxidant activity against the DPPH and ABTS radicals than that of the standard antioxidants BHA and BHT.

In vitro cytotoxic activity studies by MTT assay

The positive results obtained from the DNA binding, protein binding and antioxidative studies encouraged us to test the cytotoxicity of the complexes against a human lung cancer cell line (A549). The cytotoxicity assay for the new Pd(II) complexes was assessed using the method of MTT reduction. Cisplatin was used as a positive control. The complexes were found to be cytotoxic to lung cancer cell line (A549). The IC_{50} value (50% inhibition of cell growth for 48 h) of palladium complexes **1**, **2**, **3**, **4** and **5** are shown in Fig. 13. The new palladium complexes exhibited

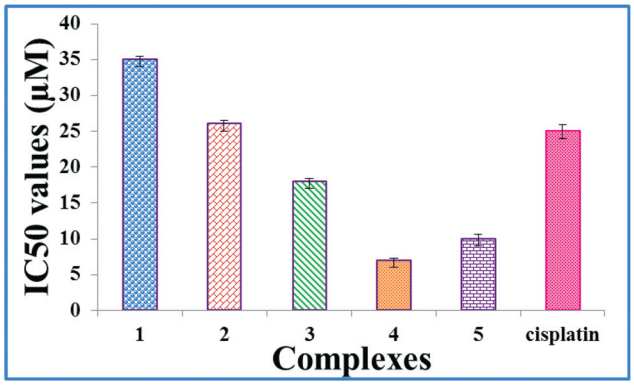

Fig. 13 The IC_{50} values (50% inhibition of cell growth for 48 h) of complexes **1–5** are depicted.

higher cytotoxic effects on lung cancer cells with lower IC_{50} values indicating its efficiency in killing the cancer cells even at low concentrations. The cytotoxic effectiveness of complexes **3**, **4** and **5** with an IC_{50} of 18, 7 and 10 μM was higher than that of cisplatin (25 μM). There are reports in the literature on the cytotoxic effects of the complexes with longer incubation time periods and such a longer incubation period may result in the development of cellular resistance for that particular complex. But, the data obtained for our complexes showed a higher cytotoxicity with a short incubation period which is highly significant when compared to the results of Beckford *et al.*[43] Furthermore, the IC_{50} values of 7 μM for complex **4** confirmed a much higher cytotoxic effect than the rest of the complexes indicating the effect of the substitution at the terminal nitrogen of the complexes for the enhanced antitumor activities.

Conclusion

Mononuclear palladium(II) complexes containing 6-methoxy-2-oxo-1,2-dihydroquinoline-3-carbaldehyde 4*N*-substituted thiosemicarbazones and triphenylphosphine have been synthesised and characterized with a view to study the effect of substitution at the terminal N of the ligand on the coordination behaviour and their biological activities. The DNA interaction and protein binding properties of the new complexes were evaluated by absorption and fluorescence spectroscopies and the results suggested that the binding affinity of the complexes increases with the increase in size of substitution at the terminal nitrogen of the thiosemicarbazone moiety. The free radical scavenging assay results showed that all the complexes possess significant activity. In addition, the *in vitro* cytotoxicity of the new complexes **1–5** was assayed against A549 cancer cell line and all the complexes exhibited good cytotoxic activity. The IC_{50} cytotoxicity values indicted that complex **4** is more cytotoxic when compared to the rest of the complexes.

Acknowledgements

Council of Scientific and Industrial Research, New Delhi, India [Grant No. 01(2216)/08/EMR-II & 21(0745)/09/EMR-II] for the financial assistance received, and the University Grants Commission, New Delhi, for the award of a Fellowship in Science for Meritorious Students (RFSMS) to E. R under the UGC-SAP-DRS programme, are gratefully acknowledged.

References

1 L. Kelland, *Nat. Rev. Cancer*, 2007, **7**, 573–584.
2 T. Boulikas and M. Vougiouka, *Oncol. Rep.*, 2003, **10**, 1663–1682.
3 E. Wong and C. M. Giandomenico, *Chem. Rev.*, 1999, **99**, 2451–2466.
4 M. Galanski, V. B. Arion, M. A. Jakupec and B. K. Keppler, *Curr. Pharm. Des.*, 2003, **9**, 2078–2089.
5 D. Wang and S. Lippard, *Nat. Rev. Drug Discovery*, 2005, **4**, 307–320.
6 J. Ruiz, N. Cutillas, C. Vicente, M. D. Villa and G. Lopez, *Inorg. Chem.*, 2005, **44**, 7365–7376.
7 E. J. Gao, C. Liu, M. C. Zhu, H. K. Lin, Q. Wu and L. Liu, *Anti-Cancer Agents Med. Chem.*, 2009, **9**, 356–368.
8 S. Padhye, Z. Afrasiabi, E. Sinn, J. Fok, K. Mehta and N. Rath, *Inorg. Chem.*, 2005, **44**, 1154–1156.
9 S. Halder, S. M. Peng, G. H. Lee, T. Chatterjee, A. Mukherjee, S. Dutta, U. Sanyal and S. Bhattacharya, *New J. Chem.*, 2008, **32**, 105–114.
10 D. K. Demertzi, M. A. Demertzis, J. R. Miller, C. S. Frampton, J. P. Jasinski and D. X. West, *J. Inorg. Biochem.*, 2002, **92**, 137–140.
11 P. I. da, S. Maia, A. G. de, A. Fernandes, J. N. Silva, A. D. Andricopulo, S. S. Lemos, E. S. Lang, U. Abram and V. M. Deflon, *J. Inorg. Biochem.*, 2010, **104**, 1276–1282.
12 A. I. Matesanz and P. Souza, *J. Inorg. Biochem.*, 2007, **101**, 245–253.
13 A. I. Matesanz, C. Hernández, A. Rodriguez and P. Souza, *J. Inorg. Biochem.*, 2011, **105**, 1613–1622.
14 L. Otero, M. Vieites, L. Boiani, A. Denicola, C. Rigol, L. Opazo, C. O. Azar, J. D. Maya, A. Morello, R. L. K. Siegel, O. E. Piro, O. E. Castellano, M. Gonzalez, D. Gambino and H. Cerecetto, *J. Med. Chem.*, 2006, **49**, 3322–3331.
15 K. Husain, M. Abid and A. Azam, *Eur. J. Med. Chem.*, 2007, **42**, 1300–1308.
16 K. Husain, M. Abid and A. Azam, *Eur. J. Med. Chem.*, 2008, **43**, 2016–2028.
17 R. Prabhakaran, P. Kalaivani, R. Jayakumar, M. Zeller, A. D. Hunter, S. V. Renukadevi, E. Ramachandran and K. Natarajan, *Metallomics*, 2011, **3**, 42–48.
18 P. Kalaivani, R. Prabhakaran, F. Dallemer, P. Poornima, E. Vaishnavi, E. Ramachandran, V. Vijaya Padma, R. Renganathan and K. Natarajan, *Metallomics*, 2012, **4**, 101–113.
19 E. Ramachandran, P. Kalaivani, R. Prabhakaran, N. P. Rath, S. Brinda, P. Poornima, V. V. Padma and K. Natarajan, *Metallomics*, 2012, **4**, 218–227.
20 P. Kalaivani, R. Prabhakaran, E. Ramachandran, F. Dallemer, G. Paramaguru, R. Renganathan, P. Poornima, V. Vijaya Padma and K. Natarajan, *Dalton Trans.*, 2012, **41**, 2486–2499.
21 D. Senthil Raja, G. Paramaguru, N. S. P. Bhuvanesh, J. H. Reibenspies, R. Renganathan and K. Natarajan, *Dalton Trans.*, 2011, **40**, 4548–4559.
22 D. Senthil Raja, N. S. P. Bhuvanesh and K. Natarajan, *Eur. J. Med. Chem.*, 2011, **46**, 4584–4594.
23 E. Ramachandran, P. Kalaivani, R. Prabhakaran, M. Zeller, J. H. Bartlett, P. O. Adero, T. R. Wagner and K. Natarajan, *Inorg. Chim. Acta*, 2012, **385**, 94–99.
24 E. Ramachandran, S. P. Thomas, P. Poornima, P. Kalaivani, R. Prabhakaran, V. V. Padma and K. Natarajan, *Eur. J. Med. Chem.*, 2012, **50**, 405–415.
25 D. Senthil Raja, N. S. P. Bhuvanesh and K. Natarajan, *Inorg. Chem.*, 2011, **50**, 12852–12866.
26 A. I. Vogel, *Text Book of Practical Organic Chemistry*, Longman, London, 5th edn, 1989, p. 268.
27 M. K. Singh, A. Chandra, B. Singh and R. M. Singh, *Tetrahedron Lett.*, 2007, **48**, 5987–5990.
28 J. L. Burmeester and F. Basolo, *Inorg. Chem.*, 1964, **3**, 1587–1593.
29 APEX2, *Program for Data Collection and Integration on Area Detectors*, BRUKER AXS Inc., 5465 East Cheryl Parkway, Madison, WI 53711-5373, USA.
30 G. M. Sheldrick, *SADABS (version 2008/1): Program for Absorption Correction for Data from Area Detector Frames*, University of Gottingen, 2008.

31 G. M. Sheldrick, *Acta Crystallogr., Sect. A: Found. Crystallogr.*, 2007, **64**, 112–122.
32 M. S. Blois, *Nature*, 1958, **181**, 1199–1200.
33 R. Re, N. Pellegrini, A. Proteggente, A. Pannala, M. Yang and C. Rice-Evans, *Free Radical Biol. Med.*, 1999, **26**, 1231–1237.
34 T. Mossman, *J. Immunol. Methods*, 1983, **65**, 55–63.
35 A. F. Tanious, D. Y. Ding, D. A. Patrick, C. Bailly, R. R. Tidwell and W. D. Wilson, *Biochemistry*, 2000, **39**, 12091–12101.
36 C. Y. Zhong, J. Zhao, Y. B. Wu, C. X. Yin and P. Yang, *J. Inorg. Biochem.*, 2007, **101**, 10–18.
37 Z. C. Liu, B. D. Wang, B. Li, Q. Wang, Z. Y. Yang, T. R. Li and Y. Li, *Eur. J. Med. Chem.*, 2010, **45**, 5353–5361.
38 A. Wolf, G. H. Shimer and T. Meehan, *Biochemistry*, 1987, **26**, 6392–6396.
39 F. J. Meyer-Almes and D. Porschke, *Biochemistry*, 1993, **32**, 4246–4253.
40 G. M. Howe, K. C. Wu and W. R. Bauer, *Biochemistry*, 1976, **19**, 339–347.
41 D. Senthil Raja, N. S. P. Bhuvanesh and K. Natarajan, *Dalton Trans.*, 2012, **41**, 4365–4377.
42 J. N. Miller, *Proc. Anal. Div. Chem. Soc.*, 1979, **16**, 203–208.
43 F. A. Beckford, M. Shaloski, G. Leblanc, J. Thessing, L. C. L. Alleyne, A. A. Holder, L. Li and N. P. Seeram, *Dalton Trans.*, 2009, 10757–10764.